Turk J Chem
35 (2011) , 375 – 391.

doi:10.3906/kim-1010-742

ZnO nanoflake arrays prepared via anodization and their performance in the photodegradation of methyl orange

Huey-Shya GOH[1], Rohana ADNAN[1,*], Muhammad Akhyar FARRUKH[2]
[1] *School of Chemical Sciences, Universiti Sains Malaysia, 11800 Penang-MALAYSIA*
e-mail: r_adnan@usm.my
[2] *Department of Chemistry, GC University Lahore, 54000 Lahore-PAKISTAN*
e-mail: akhyar100@gmail.com

Received: 20.10.2010

In the present work, anodization of zinc foil was investigated in a mixed electrolyte of ammonium sulfate and sodium hydroxide under the influence of different anodization times and concentrations of the electrolyte while the temperature and voltage were kept constant. The ZnO nanoflake arrays formed on Zn foil were characterized using a field emission scanning electron microscope (FESEM), energy dispersive X-ray spectroscopy (EDX) analysis, and X-ray diffraction (XRD). The size of the nanoflakes increased as the anodization time increased, while increasing the concentration of $(NH_4)_2SO_4$ increased the dissolution of the nanoflakes. Upon stirring, the nanoflakes that formed were more uniform and smaller in size. The catalytic activity of ZnO nanoflakes in the photodegradation of methyl orange (MO) solution under UV irradiation was evaluated. The results indicated that the surface morphology, size, and surface area of ZnO nanoflake arrays were key factors influencing the efficiency of ZnO in the photodegradation of MO.

Key Words: Anodization, zinc oxide, nanoflakes, photodegradation, methyl orange

Introduction

Zinc oxide (ZnO) is widely used in many industrial manufacturing processes, including paints, cosmetics, pharmaceuticals, plastics, batteries, electrical equipment, rubber, soap, textiles, and floor coverings, to name just a few. The interesting properties of zinc oxide have attracted the attention of many researchers in recent times. This wide band gap semiconductor (of 3.37 eV at room temperature) may have numerous possible applications, particularly in the form of thin films, nanowires, nanorods, or nanoparticles.[1] It can be used in

*Corresponding author

optoelectronic and electronic devices,[2] as well as in the field of electrochemistry for the production of chemical sensors,[3] photocatalysts,[4] and solar cells.[5] The uses of ZnO as a photocatalytic degradation material for environmental pollutants has also been extensively studied, because of its nontoxic nature, low cost, and high activity. However, such photocatalytic degradation can only proceed under UV irradiation because of its wide band gap. All kinds of novel morphologies of ZnO nanobelts,[6] nanowires,[7] nanotubes,[8] nanocombs,[9] and helical columns[10] have been synthesized. A review article written by Wang[11] suggested that ZnO probably has the most abundant forms of any known material. The properties of ZnO are strongly dependent on its structure, including the morphology, aspect ratio, size, orientation, and density of crystal.[12–14] Development of a synthesis route capable of producing ZnO nanomaterials with controlled size and morphology is important due to their potential applications as smart and functional materials.

Various methods, such as thermal evaporation,[15] hydrothermal processes,[16] microemulsion growth,[17] chemical vapor deposition (CVD),[18] and metal-organic CVD,[19] have been applied to grow ZnO nanostructures. Nevertheless, most of these methods suffer from 2 shortcomings: first, they require extreme conditions and expensive equipment; and second, they are not suitable for controllable synthesis.[20] Thus, developing room temperature approaches for fabricating ZnO nanostructures still remains a challenge.

Anodizing is an electrolytic passivation process used to increase the thickness and density of the natural oxide layer on the surface of metal parts. Besides increasing corrosion and wear resistance, anodizing is a very cost-effective method to produce uniform and adhesive oxide films on metals.[21] Anodic deposition is a process that combines simplicity, cost-effectiveness, and ease in morphology control.[22,23] Anodic films can also be used for a number of cosmetic effects, either with thick porous coatings that can absorb dyes or with thin transparent coatings that add interference effects to reflected light. Recently, much interest has been drawn toward the anodization method as it enables the preparation of nanostructured metal oxides with unique physical and chemical properties.[20,21,24–26]

Nowadays, environmental problems associated with hazardous wastes and toxic water pollutants have attracted much attention. Wastewater from textile, paper, and some other industrial processes contain residual dyes, which are nonbiodegradable. Releasing toxic and potential carcinogenic substances such as dyes into the aqueous phase creates severe environmental pollution problems. Various chemical and physical processes, such as coagulation/flocculation, activated carbon adsorption, reverse osmosis, and ultrafiltration techniques, have been developed in order to remove the color from textile effluents.[27–30] However, these techniques are nondestructive, since they only transfer the nonbiodegradable matter into sludge, giving rise to new types of pollution that need further treatment. Hence, attention has to be focused on techniques that lead to the complete destruction of the dye molecules.

Among advanced oxidation processes (AOPs), heterogeneous photocatalysis has appeared as an emerging destructive technology leading to the total mineralization of most organic pollutants. AOPs are based on the generation of reactive species such as hydroxyl radicals that oxidize a variety of organic pollutants quickly and nonselectively.[31] Semiconductor photocatalysis is a newly developed AOP, which can be conveniently applied to dye pollutants for their degradation.[32–34]

Methyl orange (MO) is an azo dye used in textiles, foodstuffs, pulp and paper, and the leather industry. Photodegradation of MO, a typical pollutant in waste water, has been investigated as a model compound under UV-Vis irradiation with different catalysts, including TiO_2/SiO_2 composite,[35] Pt-TiO_2/zeolites[36] and

N-doped TiO_2/ZnO,[37] ZnO and ZnO-SnO_2,[38–41] Ag/ZnO nanocatalyst,[42] and CuPcTs/TiO_2 catalysts.[43]

In this paper, an electrochemical process for fabricating a ZnO nanostructure under room temperature via anodic deposition of a zinc foil in a mixed ammonium sulfate ($(NH_4)_2SO_4$) and sodium hydroxide (NaOH) electrolyte is reported. The effects of different conditions of the anodization process, particularly the anodization time, concentration of the electrolyte, and stirring effect on the deposition morphology and composition, were studied. The photocatalytic activity of ZnO nanostructure arrays prepared under various anodic conditions is also presented.

Experimental

Materials and reagents

The chemical reagents used were ammonium sulfate ($(NH_4)_2SO_4$ from Merck), sodium hydroxide (NaOH from R & M Chemicals), ammonium chloride (NH_4Cl from R & M Chemicals), 99.0% zinc foil (Zn from R & M Chemicals), 99.95% platinum wire (Pt from Strem Chemicals), acetone (C_3H_6O from HmbG Chemicals), ultrapure water (produced by SG-UltraClear, 0.05 μS cm^{-1}) and methyl orange (from Laboratory LAJAX Chemicals). All chemicals were used as received without any further purification.

Fabrication of ZnO

High purity (99.0%) zinc foils with a thickness of 0.20 mm were used as a starting material in this study. The zinc foils were first degreased with acetone in an ultrasonic bath for 15 min, rinsed with ultrapure water, and dried in a nitrogen stream. Electrochemical experiments were performed using a direct current voltage source (Zhao Xin RXN-303D). The cell was a 2-electrode system consisting of zinc foil (6 cm^2) acting as the anodic electrode and platinum wire as the cathodic electrode. The distance between the anodic and cathodic electrodes was 3 cm. The electrolytes used in this process were a mixture of $(NH_4)_2SO_4$ and NaOH, $(NH_4)_2SO_4$ without NaOH, NaOH without $(NH_4)_2SO_4$, and a mixture of NH_4Cl and NaOH. Electrolyte solutions were prepared by varying the concentration of the electrolytes. All anodic deposition experiments were performed at room temperature at the potential of 10 V. After being anodized for a specific duration (30, 60, or 90 min), the foil was immediately removed from the solution and washed with ultrapure water. Finally, it was dried in an oven overnight prior to characterization. The Table shows the summary of the reaction parameters used in the preparation of anodic ZnO.

Characterization

The morphology and composition of the anodically prepared zinc oxides were characterized with a field emission scanning electron microscope (Leo Supra 50VP FESEM) equipped with energy dispersive X-ray spectroscopy (Oxford Inca 400 EDX) analysis. X-ray diffraction (XRD) was performed using an X-ray diffractometer (Siemens D5000 Kristallofex) in order to characterize the crystallinity and composition of the anodic materials. Further detail is given in our previous publications.[1]

Table. The summary of reaction parameters used in the preparation of anodic ZnO.

Parameter	Electrolyte solution	Voltage applied (V)	Anodization time (min)	Concentration
Electrolytes used	$(NH_4)_2SO_4$ + NaOH	10	90	0.0500 M $(NH_4)_2SO_4$ + 0.0250 M NaOH
	NH_4Cl + NaOH			0.0500 M NH_4Cl + 0.0250 M NaOH
	$(NH_4)_2SO_4$ without NaOH			0.0500 M $(NH_4)_2SO_4$
	NaOH without $(NH_4)_2SO_4$			0.0500 M NaOH
Anodization time	$(NH_4)_2SO_4$ + NaOH	10	30	0.0500 M $(NH_4)_2SO_4$ + 0.0250 M NaOH
			60	
			90	
Concentration of $(NH_4)_2SO_4$	$(NH_4)_2SO_4$ + NaOH	10	90	0.0250 M $(NH_4)_2SO_4$ + 0.0250 M NaOH
				0.0500 M $(NH_4)_2SO_4$ + 0.0250 M NaOH
				0.0750 M $(NH_4)_2SO_4$ + 0.0250 M NaOH
High electrolyte concentration	$(NH_4)_2SO_4$ + NaOH	10	90	1.0000 M $(NH_4)_2SO_4$ + 0.5000 M NaOH
Stirring	$(NH_4)_2SO_4$ + NaOH	10	90	0.0500 M $(NH_4)_2SO_4$ + 0.0250 M NaOH

Photocatalytic experiment

The photocatalytic degradation of methyl orange (MO) was performed using ZnO nanoflake arrays on prepared Zn substrates. The MO was used without further purification, and the initial concentration was 10 mg L^{-1}. In all experiments, the reaction temperature was kept at room temperature. Reaction suspensions were prepared by adding Zn foil, 3.0 cm^2, to 50 mL of MO aqueous solution. The reaction was performed in a 100 mL beaker under UV irradiation and vigorous stirring. Prior to irradiation, the suspension was stirred in the dark for 30 min to establish the adsorption-desorption equilibrium.[39] The suspension containing MO and the catalyst was then irradiated under UV light with a high pressure Hg lamp placed parallel to the beaker at a distance of 15 cm. An analytical sample was withdrawn (5 mL) from the reaction suspension every 15 min and filtered. The absorbance of the filtrate was then measured with a UV spectrophotometer (US-H10 Optical Modulex) at a wavelength of 469 nm. The blank experiment was conducted in the presence of irradiation without a photocatalyst.

Results and discussion

Surface morphology of the anodized ZnO nanoflake arrays

The formation of the ZnO nanoflake arrays in the $(NH_4)_2SO_4$ and NaOH mixture initially occurred through the dissolution of Zn in the electrolyte solution, leading to the formation of a zinc ion complex deposited onto the surface of the anode and finally the formation of ZnO. As reported in most studies, the possible mechanism for the process can be expressed as follows:[20,44]

$$Zn \rightarrow Zn^{2+} + 2e^- \quad (1)$$

$$Zn^{2+} + 4OH^- \rightarrow Zn(OH)_4^{2-}\ (aq) \quad (2)$$

$$Zn(OH)_4^{2-}\ (aq) \rightarrow Zn(OH)_2\,(s) + 2OH^- \quad (3)$$

$$2Zn(OH)_2\ (s) \rightarrow 2ZnO\ (s) + 2H_2O\ (aq) \quad (4)$$

The initial stage of the reaction is the active dissolution of Zn in Eq. (1), which is attributed to the formation of $Zn(OH)_4^{2-}$ in Eq. (2). When the concentration of $Zn(OH)_4^{2-}$ exceeds the solubility product of $Zn(OH)_2$, precipitation of a compact layer of $Zn(OH)_2$ will occur on the anode surface, as in Eq. (3). Lastly, ZnO will form, as in Eq. (4). The presence of SO_4^{2-} will stimulate the active dissolution of Zn. This is ascribed to its adsorption on the metal surface and subsequent participation in the oxidation of the metal atoms.[44] This will lead to the formation of water soluble zinc sulfate, which is an intermediate product for the dissolution of zinc and zinc oxide during the anodization.[45]

Effect of different electrolytes

In general, it appears that the electrochemical condition is an important factor for the formation of nanoflake arrays. When using different electrolytes for the anodization of zinc foil and while keeping other parameters constant, different ZnO nanostructured arrays were observed. As shown in Figure 1, in an electrolyte of 0.0500 M NH_4Cl with 0.0250 M NaOH (Figure 1a), a ZnO nanoparticle array was formed, whereas in 0.0500 M NaOH (Figure 1b), a ZnO nanoflower array was observed. Figures 1c and 1d show images of the ZnO nanoflake arrays grown by anodization of zinc foil in 0.0500 M $(NH_4)_2SO_4$ without NaOH, and 0.0500 M $(NH_4)_2SO_4$ with 0.0250 M NaOH, respectively. This result is similar to that reported by Kim and Choi,[45] who obtained ZnO polygonal flakes perpendicular to the surface through anodization of Zn foil in ethanolic H_2SO_4. In terms of nanoflake size, Figure 1c shows smaller and nonuniform nanoflakes compared to those shown in Figure 1d, which were formed with the addition of NaOH. This shows that the addition of NaOH also affects the nanoflake size due to the presence of OH^- ions, which contribute to the formation of ZnO.[20] In the absence of NaOH, nanoflakes of various sizes were formed. This study further confirms that different types of electrolytes produce different morphologies of ZnO.

Effect of anodization time

Figure 2 shows the FESEM micrographs of the ZnO nanoflake arrays prepared by anodization of zinc foil at 10 V in a mixture of 0.0500 M $(NH_4)_2SO_4$ and 0.0250 M NaOH electrolytes at room temperature using different anodization times. At 30 min (Figure 2a), incomplete formation of tiny nanoflake structure was observed, while

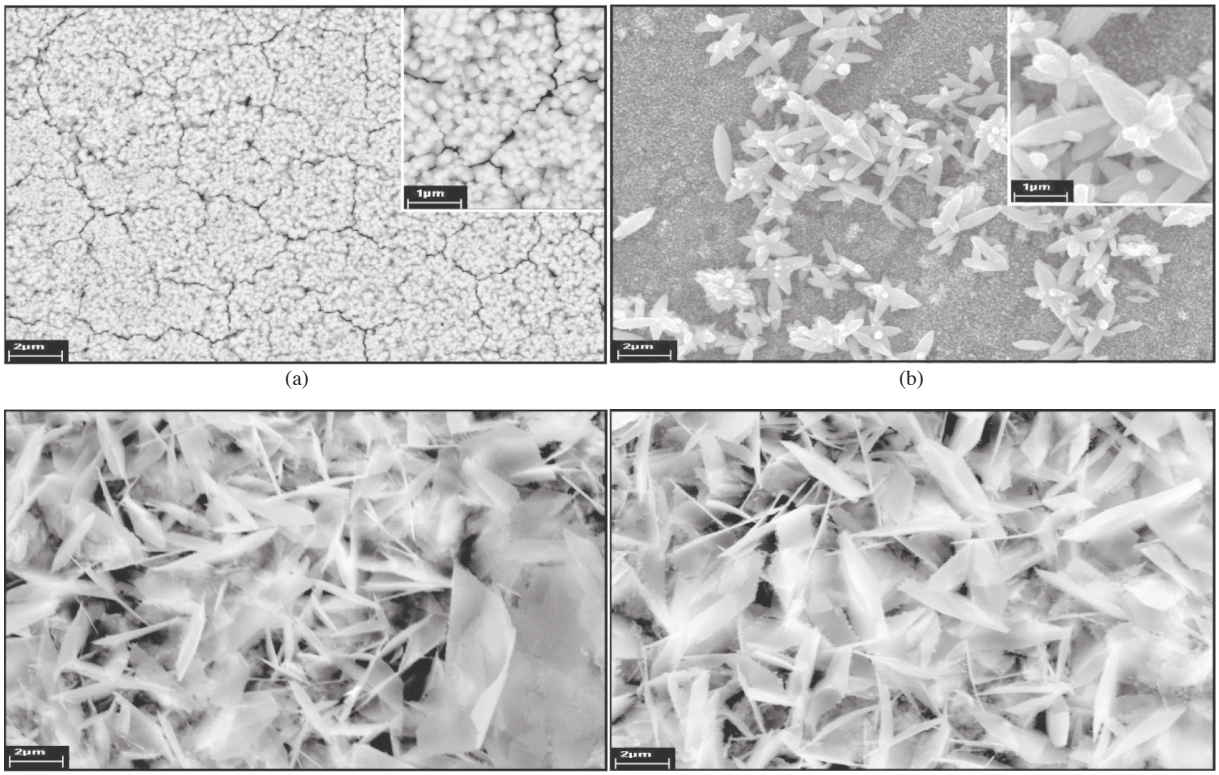

Figure 1. FESEM images of zinc foil anodized at 10 V in electrolytes: a) 0.0500 M NH_4Cl + 0.0250 M NaOH, b) 0.0500 M NaOH, c) 0.0500 M $(NH_4)_2SO_4$, and d) 0.0500 M $(NH_4)_2SO_4$ + 0.0250 M NaOH, at room temperature for 90 min [5000× magnification] (inset micrographs show images at 10,000× magnification).

60 min (Figure 2b) and 90 min (Figure 1d) of anodization showed a more complete formation of nanoflake arrays. The size of nanoflakes increased as the anodization time increased. The nanoflake arrays formed after 90 min was more packed and uniform compared to the one prepared at 60 min. This indicates that anodization time plays a role in the determination of nanoflake size and distribution. Furthermore, the effect of stirring during the anodization reaction was also studied. Figure 2c shows the ZnO nanoflake arrays prepared by anodization of zinc foil at room temperature and 10 V for 90 min with mild stirring in 0.0500 M $(NH_4)_2SO_4$ and 0.0250 M NaOH electrolytes. It can be observed that with stirring, the nanoflakes that formed were more uniform and smaller in size. The reaction was faster with stirring as a result of the well-distributed OH^- ions inside the electrolyte solution. However, the ZnO formed will redissolve due to stirring, which prevents it from growing into larger nanoflakes. Kim and Choi[45] also studied the effect of stirring, and their results indicated that the anodization process with and without stirring gave different morphologies of ZnO. They reported that randomly oriented flakes were formed without stirring.

Effect of $(NH_4)_2SO_4$ concentration

The effect of different concentrations of $(NH_4)_2SO_4$ used in the electrolyte was studied. Figure 3 shows the FESEM images of the ZnO nanoflake arrays prepared by anodization of zinc foil at 10 V for 90 min in 0.0250

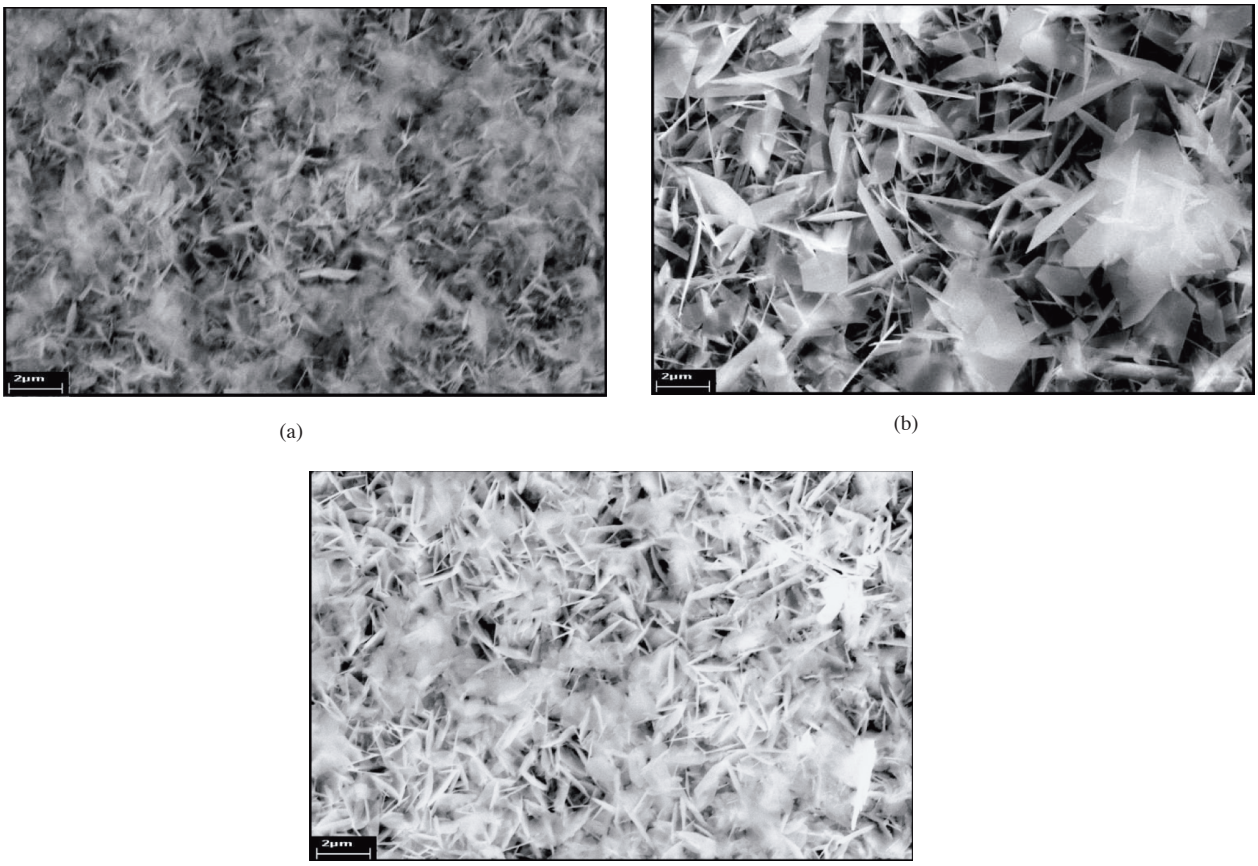

(a) (b)

(c)

Figure 2. FESEM images of zinc foil anodized at 10 V in 0.0500 M $(NH_4)_2SO_4$ and 0.0250 M NaOH electrolyte mixture at room temperature using different anodization times: a) 30 min, b) 60 min, and c) 90 min (with stirring) [5000× magnification].

M NaOH and different concentrations of $(NH_4)_2SO_4$. At a lower $(NH_4)_2SO_4$ concentration (0.0250 M), the formation of nanoflakes was incomplete; Figure 3a shows that the particles joined together to form the nanoflakes arrays. By increasing the $(NH_4)_2SO_4$ concentration to 0.0500 M (Figure 1d), a nondirectional nanoflake array was formed. Nevertheless, as the concentration of $(NH_4)_2SO_4$ increased to 0.0750 M, the ZnO nanoflakes that formed (Figure 3b) seemed to have undergone dissolution due to the possible formation of a zinc sulfate intermediate as the concentration of SO_4^{2-} in the electrolyte increased. This indicates that the concentration of $(NH_4)_2SO_4$ will affect the morphology of the ZnO formed. Figure 3c shows an image of the ZnO formed when even higher concentrations of $(NH_4)_2SO_4$ and NaOH were used. The nanoflakes aligned themselves in an orderly manner, forming a layer. We believe that although the increase of the concentration of SO_4^{2-} in the electrolyte will lead to a greater dissolution effect such as that in 0.0750 M $(NH_4)_2SO_4$, the increase in the OH^- ions in the electrolyte will promote the formation of ZnO.[44] These 2 effects will cancel each other and hence the formation of nanoflake arrays can still be observed.

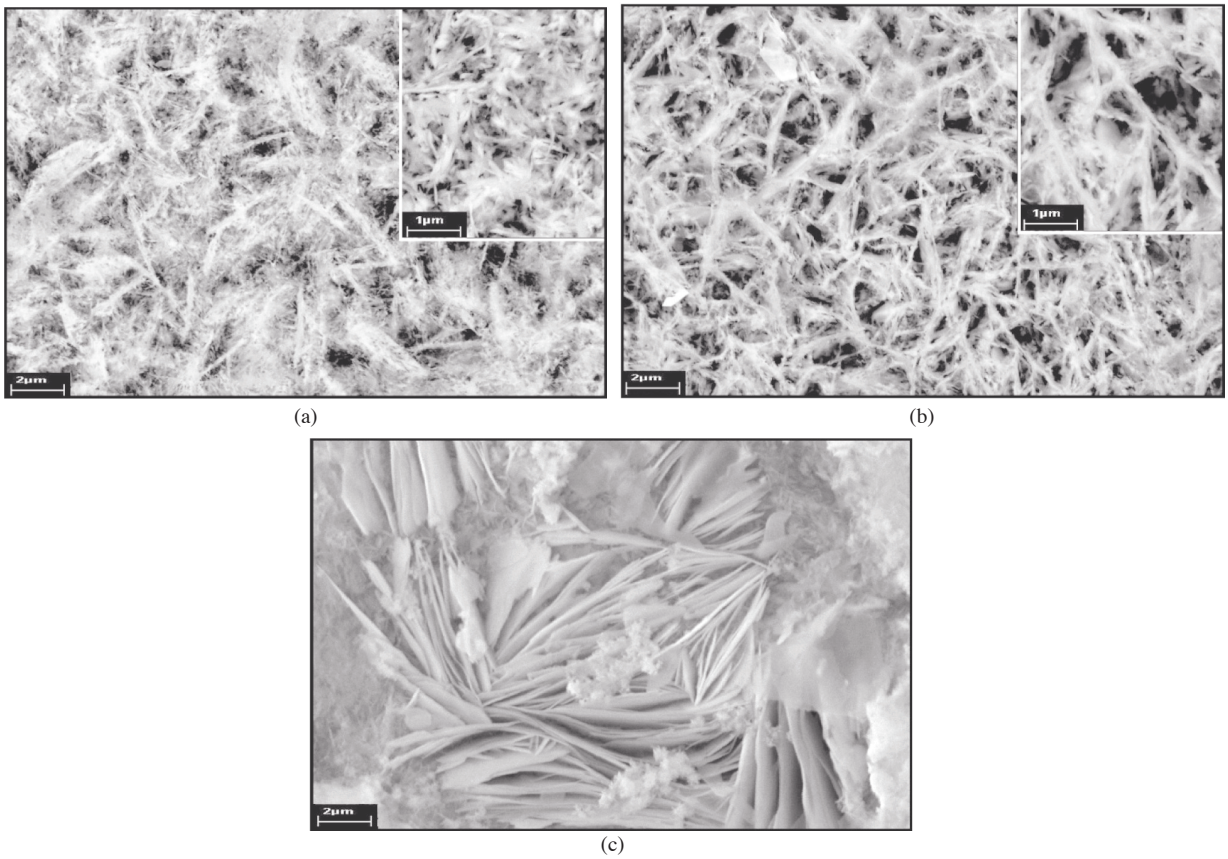

Figure 3. FESEM images of zinc foil anodized at 10 V in 0.0250 M NaOH electrolyte and different concentrations of $(NH_4)_2SO_4$: a) 0.0250 M, b) 0.0750 M, and c) 1.0000 M $(NH_4)_2SO_4$ + 0.5000 M NaOH, at room temperature for 90 min [5000× magnification] (inset micrographs show images at 10,000× magnification).

EDX analysis

Chemical stoichiometry of the nanoflakes formed in an electrolyte mixture of $(NH_4)_2SO_4$ and NaOH was investigated using energy dispersive X-ray (EDX) analysis, and the results are shown Figure 4. The results, as shown in Figures 4a ($(NH_4)_2SO_4$ + NaOH) and Figure 4d ($(NH_4)_2SO_4$), indicated the presence of sulfur besides zinc and oxygen. This suggests the presence of impurity, such as SO_4^{2-} ions, from the electrolyte solution. On the other hand, the EDX analysis of nanostructure arrays formed in the NaOH electrolyte (Figure 4b) and a mixture of NH_4Cl and NaOH (Figure 4c) indicated the presence of only carbon, zinc, and oxygen. The presence of carbon may be due to the double-sided tape used to attach the sample during the scanning process. The nanostructure array's approximately 1:1 atomic ratio of zinc to oxygen suggested that the ZnO formed was nearly pure.

XRD analysis

The crystalline phase of the nanoflakes was assessed by conducting XRD measurements. Figure 5 shows the XRD patterns of the samples anodized in different electrolytes. The diffraction peaks at 2θ values of 31.77°,

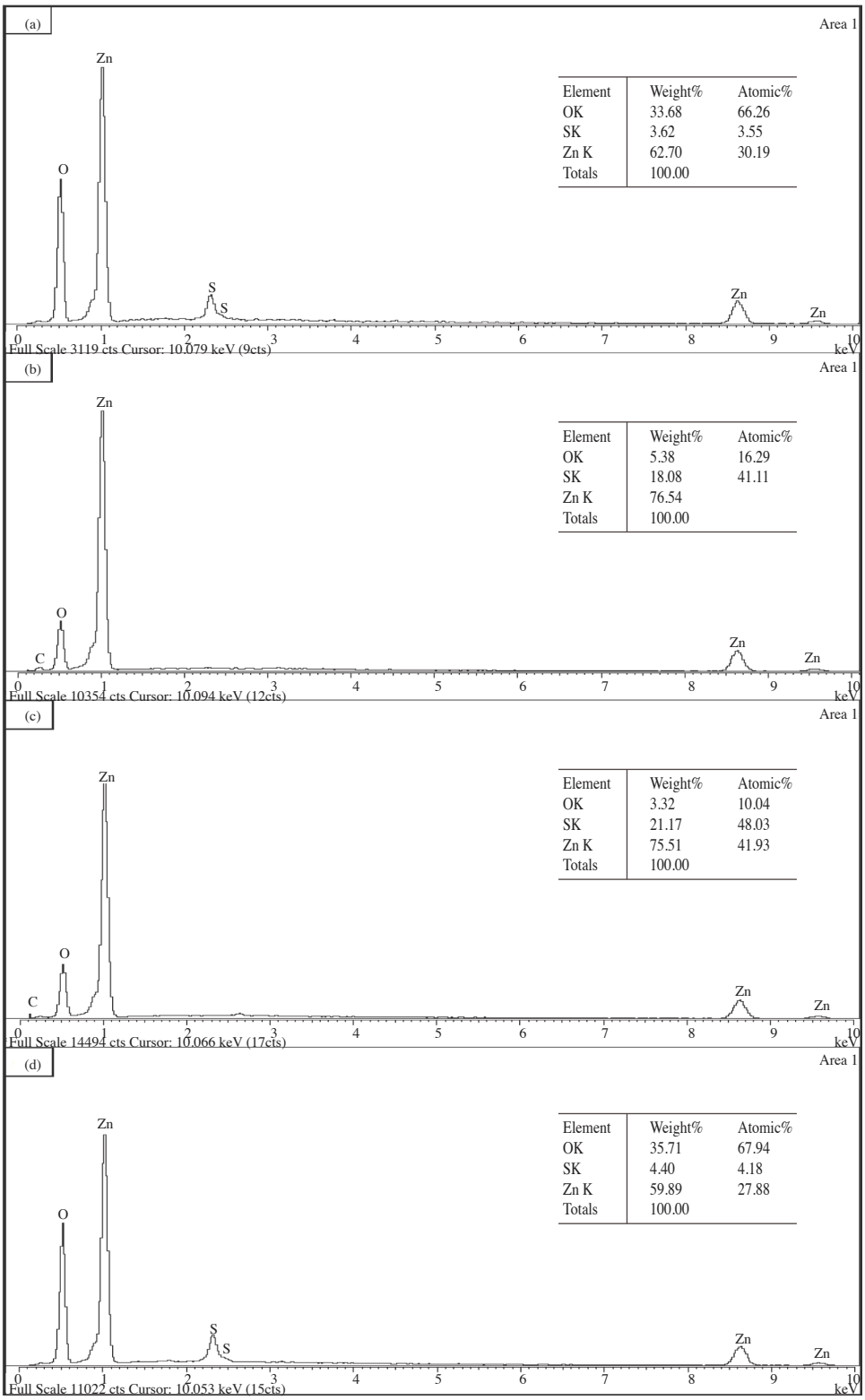

Figure 4. EDX spectra for ZnO formed in different electrolytes: a) $(NH_4)_2SO_4$ + NaOH, b) NaOH, c) NH_4Cl + NaOH, and d) $(NH_4)_2SO_4$.

34.42°, 36.25°, 47.54°, 56.60°, 62.86°, 66.38°, 67.96°, 69.10°, 72.56°, 76.95°, and 81.37° corresponded to the (100), (002), (101), (102), (110), (103), (200), (112), (201), (004), (202), and (104) planes of hexagonal ZnO, respectively (JCPDS 36-1451). Other peaks corresponded to pure zinc (JCPDS 65-3358), which clearly originated from the foil. The XRD patterns for electrolytes containing $(NH_4)_2SO_4$ did not show the presence of SO_4^{2-}. This suggests that there may have been just a trace of impurities present on the foil, as the atomic percentage of sulfur shown in EDX analysis was quite low. The XRD patterns of samples prepared in an electrolyte of only NaOH solution and a mixture of NH_4Cl and NaOH also showed the same pattern. This suggests that the same products (ZnO) were formed using these electrolytes.

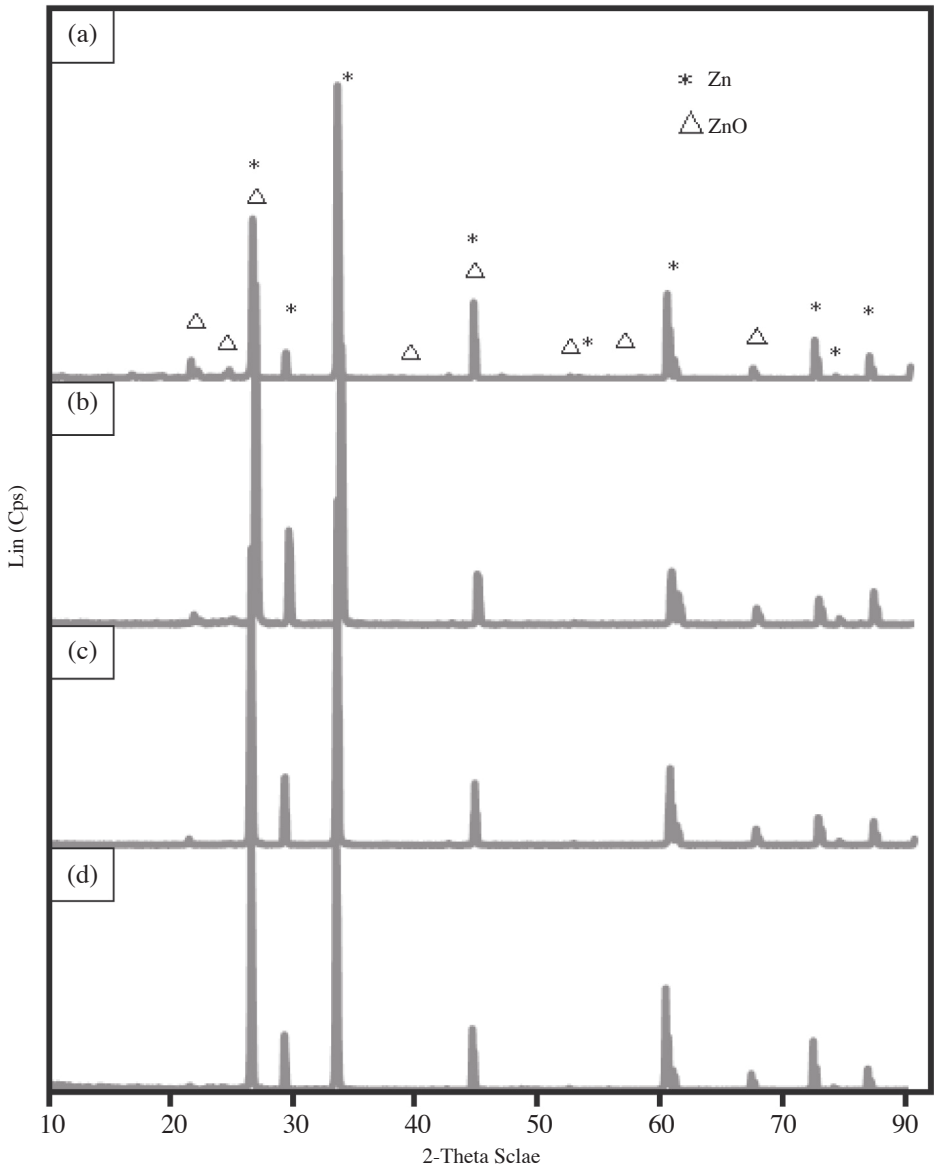

Figure 5. XRD patterns of zinc foil anodized in different electrolytes: a) $(NH_4)_2SO_4$ + NaOH, b) NH_4Cl + NaOH, c) NaOH, and d) $(NH_4)_2SO_4$.

Photocatalytic degradation of methyl orange

The photocatalytic activities of ZnO nanoflakes produced under different anodic conditions were used for the photodegradation of MO in aqueous solution. The absorbance of the analytical samples withdrawn from the reaction suspension every 15 min was measured at λ_{max} 469 nm to determine the concentration of MO. The decomposition rate or degradation rate was calculated using the following equation:[20,44]

Degradation rate = $(1 - c/c_{eq}) \times 100\%$.

Figures 6a-6c show the results for the photocatalytic activity of ZnO toward MO under different conditions. The photodegradation of MO was performed in a blank, without using ZnO, as displayed in Figure 6a (blank), which shows the straight line indicating that MO cannot be degraded under this condition. However, the presence of ZnO nanoflake arrays shows the effective photocatalytic degradation of MO.

Effect of anodization time on photocatalytic activity

Under different anodization times, the morphology of the ZnO formed on the Zn foil was different. This will affect the photodegradation of MO in aqueous solution. In Figure 6a, it can be clearly observed that the ZnO formed after an anodization time of 30 min showed poor degradation (9.17% degradation after 1 h), as compared to 60 min (14.83% degradation after 1 h) or 90 min (12.40% degradation after 1 h). Among them, the anodization time of 60 min showed the highest photodegradation ability. The enhancement of the photocatalytic activity may be due to the different surface structure. As shown in Figure 2a, the ZnO formed after 30 min showed incomplete formation of tiny nanoflake structures, whereas those anodized after 60 min (Figure 2b) and 90 min (Figure 1d) showed a more complete formation of nanoflake arrays. Owing to this incomplete formation, the ZnO formed after 30 min of anodization had less surface area than those after 60 min or 90 min. The ZnO formed after 60 min performed better in photocatalytic reactions than that formed after 90 min. This may be because the ZnO nanoflakes that formed after 90 min were thicker, and fewer nanoflakes were formed, although the size was larger compared to that after 60 min. Thus, the surface area was less and the photodegradation ability was also reduced. Sreekantan et al.[46] conducted studies on the photodegradation of MO using anatase-rutile TiO_2 nanotubes produced via anodization at different voltages. Their results indicated that upon varying the applied voltage, different surface structures were formed. TiO_2 with a tubular structure had a larger surface area, which enhanced the photocatalytic activity.

Effect of concentration of $(NH_4)_2SO_4$ on photocatalytic activity

The performance of the photodegradation of MO using the ZnO that was synthesized in electrolytes of different $(NH_4)_2SO_4$ and NaOH concentrations (Figure 6b) can also be explained in terms of the different surface structure. In Figure 3a, the FESEM image of the ZnO nanoflake arrays formed in the electrolyte with 0.0250 M $(NH_4)_2SO_4$ shows that the formation of nanoflakes remained incomplete. At this stage, the nanoparticles started to join up to form the nanoflake arrays. These tiny nanoparticles were agglomerated and hence had a lower surface area compared to nanoflake arrays formed through anodization in the electrolyte with 0.0500 M $(NH_4)_2SO_4$ (Figure 1d) (12.40% degradation after 1 h). Thus, it had poorer degradation (10.72% degradation after 1 h) due to its lower surface area (Figure 3a). At 0.0750 M $(NH_4)_2SO_4$ (Figure 3b), active dissolution of ZnO nanoflakes occurred. This formless structure possessed even less surface area than that from the 0.0250

M $(NH_4)_2SO_4$. As a result, it showed the poorest photodegradation of MO (10.59% degradation after 1 h). A layer structure formed (Figure 3c) upon increasing both the concentrations of $(NH_4)_2SO_4$ (1.000 M) and NaOH (0.500 M). This type of surface structure has a large contribution to the photodegradation performance (18.37% degradation after 1 h). The photodegradation efficiency of this sample was found to be the highest due to the formation of a layer structure, which increased the surface area and enhanced the photocatalytic activity of ZnO.

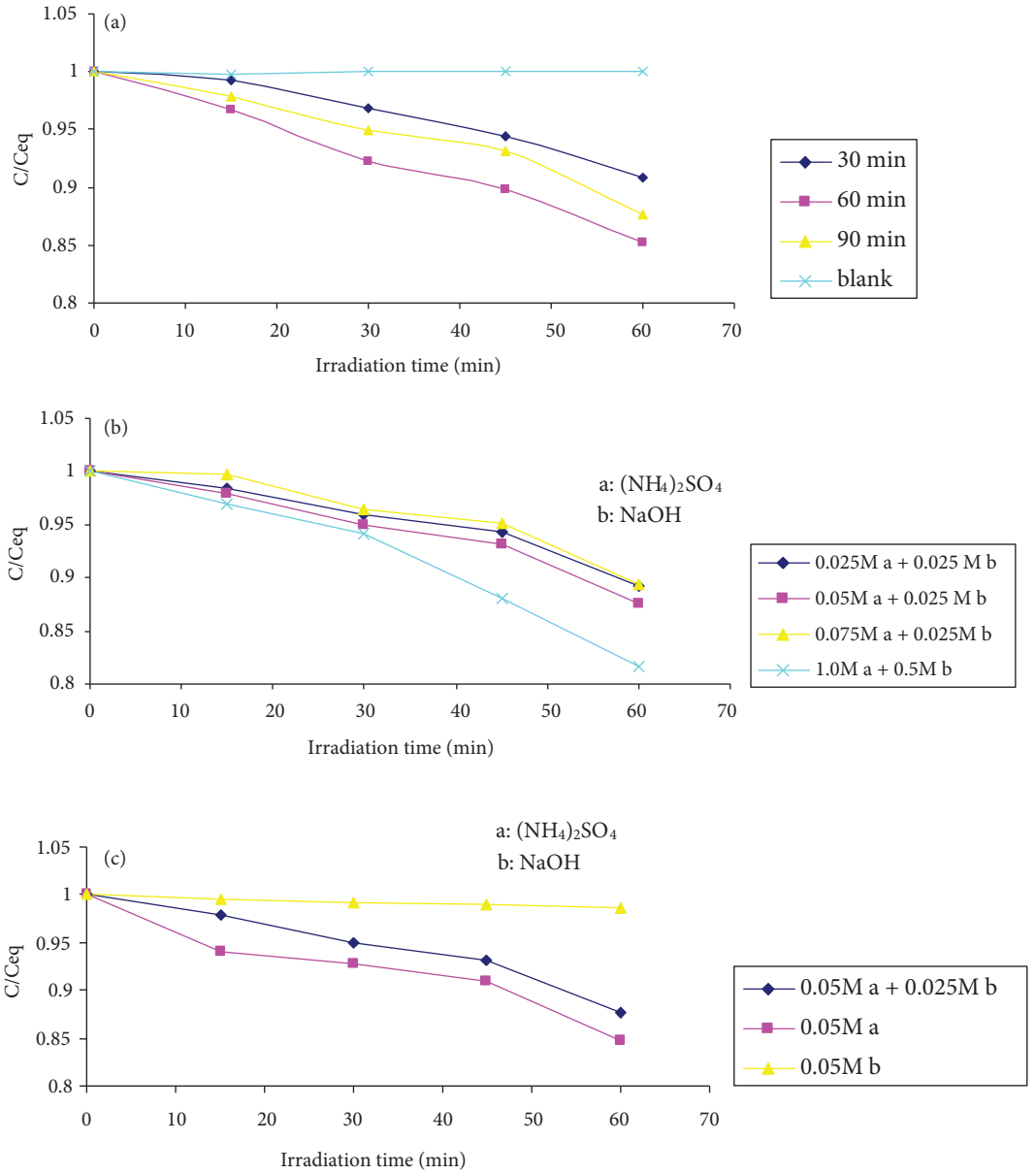

Figure 6. Effect of different parameters on photocatalytic activity of ZnO on methyl orange: a) anodization time, b) concentration of $(NH_4)_2SO_4$, and c) different electrolytes.

Effect of different electrolytes on photocatalytic activity

Figure 6c shows the result of the photodegradation of MO using ZnO produced in different electrolytes. As shown in Figure 1b, in 0.0500 M NaOH, a ZnO nanoflower array was observed, whereas ZnO prepared in 0.0500 M $(NH_4)_2SO_4$ without NaOH (Figure 1c) and in 0.0500 M $(NH_4)_2SO_4$ with 0.0250 M NaOH (Figure 1d) showed the growth of ZnO nanoflake arrays. The nanoflowers that formed were fewer in quantity, although the size was smaller, and thus they were lower in surface area compared to the nanoflakes. This explains the photodegradation performance of MO for these 3 samples, where the Zn substrate with ZnO nanoflowers had poorer photocatalytic efficiency (1.45% degradation after 1 h) than the ZnO nanoflakes. Zhang et al.[39] studied the photocatalytic reaction of MO using a nanometer coupled oxide, ZnO-SnO_2, prepared via the coprecipitation method, and reported that the presence of SO_4^{2-} anions exerted an inhibitive effect on the photodegradation process due to the competitive adsorption between SO_4^{2-} and MO at the photocatalyst surface. EDX analysis showed the presence of SO_4^{2-} in the ZnO nanoflake arrays that were formed using an electrolyte containing sulfate anions. However, the results of photodegradation of MO revealed that the presence of SO_4^{2-} anions did not show much inhibitive effect due to their trace quantity. This is consistent with the XRD analysis, in which the presence of trace SO_4^{2-} was undetectable. ZnO formed in a NaOH electrolyte (basic solution) showed poor degradation of MO. The photocatalytic activity can be explained in terms of the electrostatic interactions between the catalyst surface and the MO anions.[40] Higher pH values may induce the formation of a highly negative charged oxide surface, thus producing higher electrostatic repulsion between the MO anion (pK_1 = 3.46) and the oxide surface.[41]

After 1 h, the Zn foil that was anodized in 0.050M $(NH_4)_2SO_4$ without NaOH degraded the MO solution to the same degree as that of ZnO formed with an anodization time of 60 min in a mixture of 0.0500 M $(NH_4)_2SO_4$ and 0.0250 M NaOH. The percentages of degradation of MO after 1 h were 15.21% and 14.83%, respectively. This suggests that both of them had almost the same photocatalytic efficiency, although initially the former performed better than the latter. In terms of morphology, both showed nanoflakes of almost similar size and thickness. Hence, this explains why the ZnO produced in 0.0500 M $(NH_4)_2SO_4$ performed better than that produced in 0.0500 M $(NH_4)_2SO_4$ with 0.0250 M NaOH (12.40% degradation after 1 h) for the same anodization time (90 min). In terms of pH value, the ZnO formed in an electrolyte of 0.050M $(NH_4)_2SO_4$ without NaOH exhibited higher photocatalytic activity than that with NaOH. The results pertaining to photodegradation in terms of percentage as a function of different irradiation times, concentrations, and electrolytes are displayed in Figures 7a-7c.

Pseudo-first-order rate constants, with k for the photodegradation of MO using ZnO catalysts synthesized under different anodic conditions, are shown in Figures 8a-8c. In terms of anodization time, the ZnO formed using an anodization time of 60 min gave the highest k value, 0.0263 min^{-1}. In terms of concentrations, ZnO produced using a high concentration of $(NH_4)_2SO_4$ and 0.500 M NaOH showed the highest k value (0.0225 min^{-1}). ZnO synthesized in a NaOH solution showed the highest rate constant value, 0.0285 min^{-1}, compared to those formed in other electrolyte solutions. These k values are among the highest reported. Wang et al.[41] reported a pseudo-first-order rate constant value of approximately $\sim$ 0.015 min^{-1} for ZnO synthesized via the coprecipitation method. Meanwhile, Zhang et al.[39] who used the same method of preparation but employed $NH_3.H_2O$ as a precipitant instead of $LiOH.H_2O$, reported a first-order rate constant for the first 15 min

of irradiation of 0.0335 min^{-1}. Kansal et al.,[31] who studied the photocatalytic degradation of MO using various semiconductors such as TiO_2, ZnO, SnO_2, ZnS, and CdS, reported that the first-order rate constant for photocatalytic decolorization of MO in aqueous ZnO was calculated to be 2.9×10^{-4} s^{-1} (0.0174 min^{-1}).

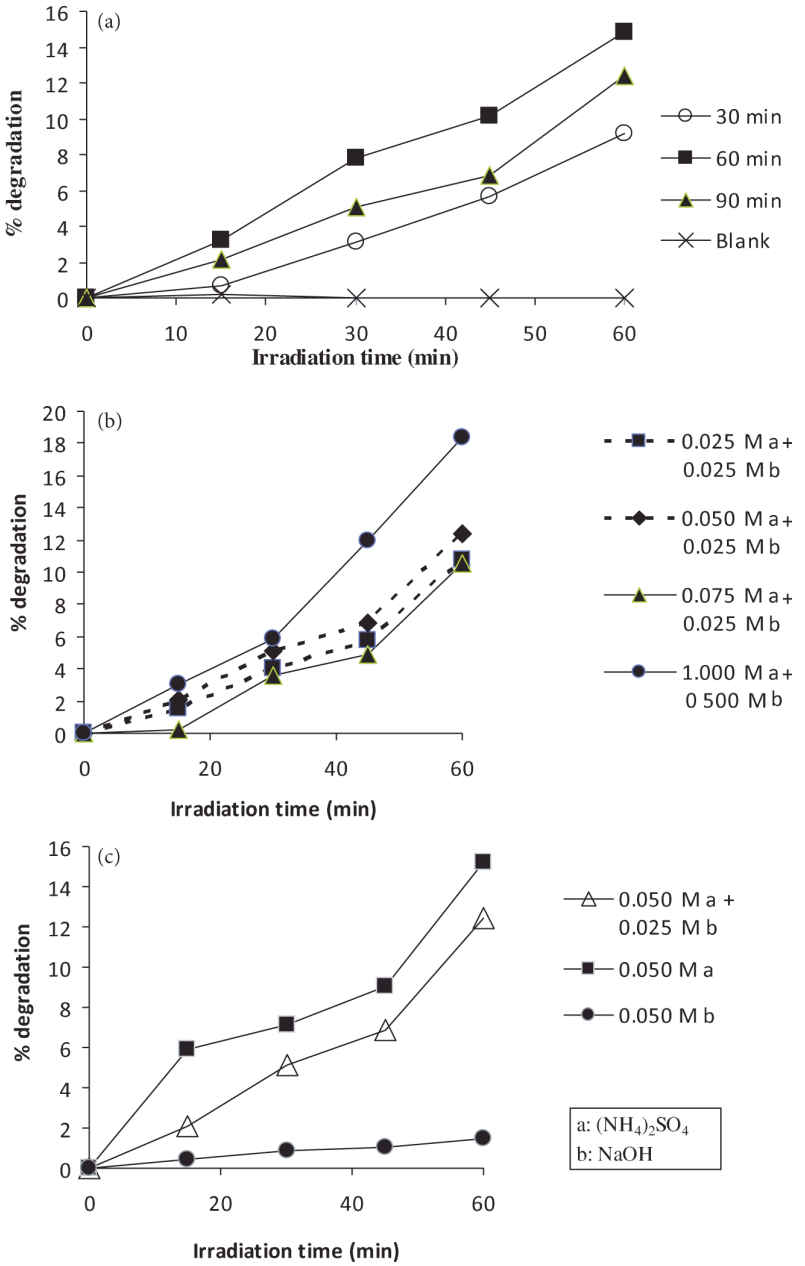

Figure 7. Photodegradation percentage as a function of irradiation time at different: a) anodization times, b) concentrations of $(NH_4)_2SO_4$, and c) electrolytes.

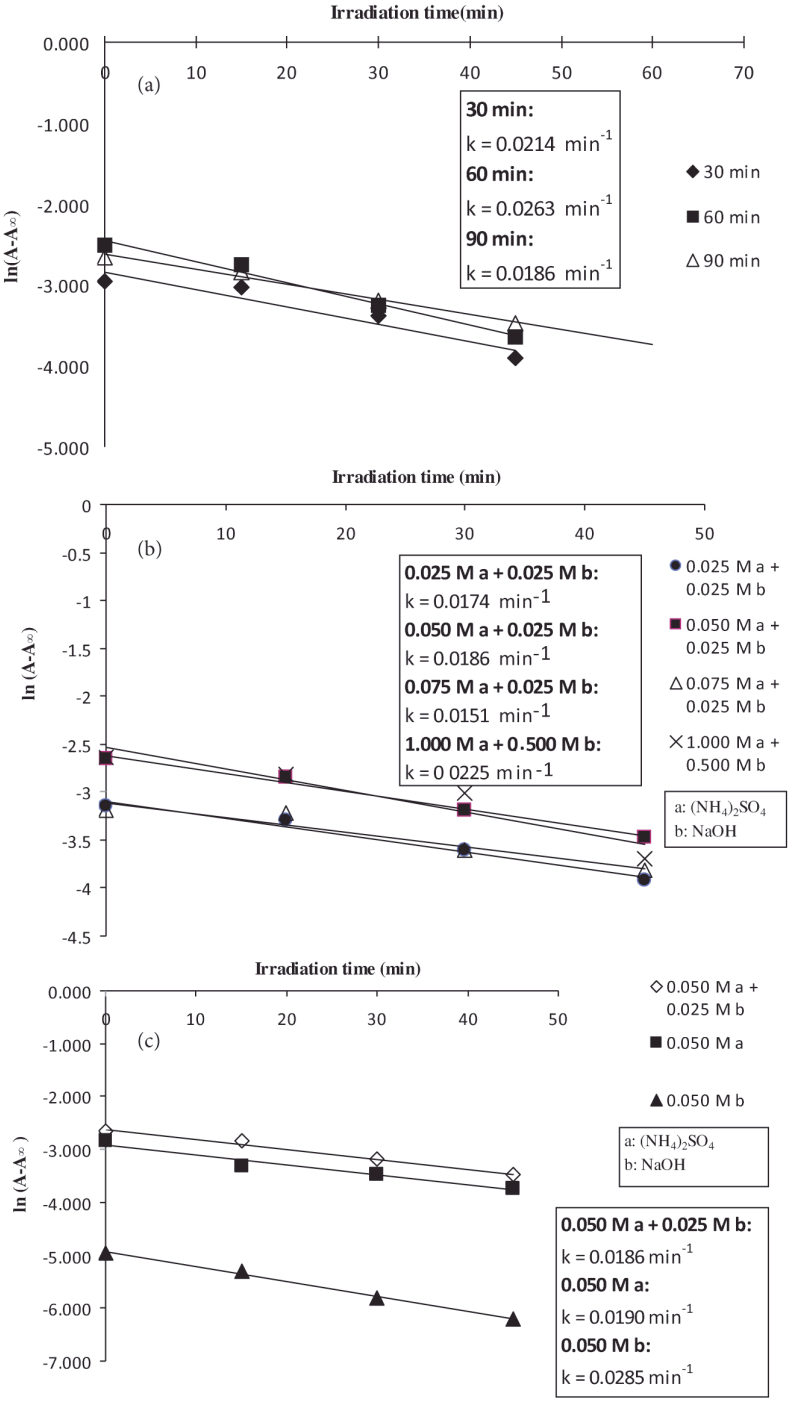

Figure 8. Pseudo-first-order plot of $\ln(A_t\text{-}A_\infty)$ as a function of irradiation time at different: a) anodization times, b) concentrations of $(NH_4)_2SO_4$, and c) electrolytes.

Conclusions

In conclusion, ZnO of various nanostructures and sizes was successfully prepared via anodization of Zn foil under different anodic conditions. The morphology of ZnO was found to be affected by anodization time, concentration of electrolyte, electrolytes used, and stirring effects. ZnO nanoflakes were formed in a mixture of $(NH_4)_2SO_4$ and NaOH electrolytes. The size of the nanoflakes increased as the anodization time increased. More uniform but smaller nanoflakes formed upon stirring. Increasing the concentration of $(NH_4)_2SO_4$ increased the dissolution of nanoflakes. EDX and XRD analyses confirmed the formation of hexagonal ZnO. The efficiency of the photodegradation of MO depends on the surface morphology, size, and surface area of ZnO. With anodization of 1 h in the presence of a mixture of 0.075 M $(NH_4)_2SO_4$ and 0.025 M NaOH, the surface area was found to be lower, with the least photocatalytical activity of 10.59%. The photocatalytical activity was found to be highest (18.37%) in 1.0 M $(NH_4)_2SO_4$ and 0.5 M NaOH due to the increase in surface area. The results were also verified with kinetics data, with the first-order rate constant values of 0.0151 and 0.0225 min^{-1}, respectively, showing the highest activity reported in the literature. The activity of ZnO prepared in 0.05 M NaOH was found to be higher than that of all of the samples mentioned above, with a first-order rate constant value of 0.0285 min^{-1}.

Acknowledgement

The authors gratefully acknowledge Universiti Sains Malaysia and the Malaysian government for financial support through a short-term research grant (1001/PKIMIA/815060).

References

1. Yazid, H.; Adnan, R.; Hamid, S. A.; Farrukh, M. A. *Turk. J. Chem.* **2010**, *34*, 639-650.
2. Huang, M.; Wu, Y.; Feick, H.; Tran, N.; Weber, E.; Yang, P. *Adv. Mater.* **2001**, *13*, 113-116.
3. Weißenrieder, K.; Müller, J. *Thin Solid Films* **1997**, *300*, 30-41.
4. Anpo, M.; Chiba, K.; Tomonari, M.; Coluccia, S.; Che, M.; Fox, M. *B. Chem. Soc. Jpn.* **1991**, *64*, 543-551.
5. Yoshida, T.; Terada, K.; Schlettwein, D.; Oekermann, T.; Sugiura, T.; Minoura, H. *Adv. Mater.* **2000**, *12*, 1214-1217.
6. Pan, Z.; Dai, Z.; Wang, Z. *Science* **2001**, *291*, 1947.
7. Singjai, P.; Jintakosol, T.; Singkarat, S.; Choopun, S. *Mater. Sci. Eng. B* **2007**, *137*, 59-62.
8. Zhang, J.; Sun, L.; Liao, C.; Yan, C. *Chem. Commun.* **2002**, *2002*, 262-263.
9. Yan, H.; He, R.; Johnson, J.; Law, M.; Saykally, R.; Yang, P. *J. Am. Chem. Soc.* **2003**, *125*, 4728-4729.
10. Tian, Z.; Voigt, J.; Liu, J.; McKenzie, B.; McDermott, M. *J. Am. Chem. Soc.* **2002**, *124*, 12954-12955.
11. Wang, Z. *Mater. Today* **2004**, *7*, 26-33.
12. Zhang, J.; Sun, L.; Yin, J.; Su, H.; Liao, C.; Yan, C. *Chem. Mater.* **2002**, *14*, 4172-4177.
13. Wang, Z. *J. Phys-Condens. Mat.* **2004**, *16*, R829.

14. Zhao, Q.; Zhang, H.; Zhu, Y.; Feng, S.; Sun, X.; Xu, J.; Yu, D. *Appl. Phys. Lett.* **2005**, *86*, 203115.
15. Umar, A.; Kim, S.; Kim, J.; Al-Hajry, A.; Hahn, Y. *J. Alloy. Comp.* **2008**, *463*, 516-521.
16. Jang, J.; Kim, C.; Ryu, H.; Razeghi, M.; Jung, W. *J. Alloy. Comp.* **2008**, *463*, 503-510.
17. Guo, L.; Ji, Y.; Xu, H.; Simon, P.; Wu, Z. *J. Am. Chem. Soc.* **2002**, *124*, 14864-14865.
18. Wu, C.; Chang, L.; Chen, H.; Lin, C.; Chang, T.; Chao, Y.; Yan, J. *Thin Solid Films* **2006**, *498*, 137-141.
19. Park, J.; Oh, H.; Kim, J.; Kim, S. *J. Cryst. Growth* **2006**, *287*, 145-148.
20. Sreekantan, S.; Gee, L.; Lockman, Z. *J. Alloy. Comp.* **2009**, *476*, 513-518.
21. Kim, S.; Lee, J.; Choi, J. *Electrochim. Acta* **2008**, *53*, 7941-7945.
22. Wang, F.; Liu, R.; Pan, A.; Cao, L.; Cheng, K.; Xue, B.; Wang, G.; Meng, Q.; Li, J.; Li, Q. *Mater. Lett.* **2007**, *61*, 2000-2003.
23. Lin, C.; Lin, H.; Li, J.; Li, X. *J. Alloy. Comp.* **2008**, *462*, 175-180.
24. Zhang, H.; Quan, X.; Chen, S.; Zhao, H. *Appl. Phys. A* **2007**, *89*, 673-679.
25. Huang, G.; Wu, X.; Cheng, Y.; Shen, J.; Huang, A.; Chu, P. *Appl. Phys. A-Mater.* **2007**, *86*, 463-467.
26. He, S.; Zheng, M.; Yao, L.; Yuan, X.; Li, M.; Ma, L.; Shen, W. *Appl. Surf. Sci.* **2010**, *256*, 2557-2562.
27. Al-Bastaki, N. *Chem. Eng. Process.* **2004**, *43*, 1561-1567.
28. Ahmad, A.; Puasa, S.; Zulkali, M. *Desalination* **2006**, *191*, 153-161.
29. Gomez, V.; Larrechi, M.; Callao, M. *Chemosphere* **2007**, *69*, 1151-1158.
30. Szygula, A.; Guibal, E.; Palacín, M.; Ruiz, M.; Sastre, A. *J. Environ. Manage.* **2009**, *90*, 2979-2986.
31. Kansal, S.; Singh, M.; Sud, D. *J. Hazard. Mater.* **2007**, *141*, 581-590.
32. Lachheb, H.; Puzenat, E.; Houas, A.; Ksibi, M.; Elaloui, E.; Guillard, C.; Herrmann, J. *Appl. Catal. B: Environ.* **2002**, *39*, 75-90.
33. Chakrabarti, S.; Dutta, B. *J. Hazard. Mater.* **2004**, *112*, 269-278.
34. Bizani, E.; Fytianos, K.; Poulios, I.; Tsiridis, V. *J. Hazard. Mater.* **2006**, *136*, 85-94.
35. Xu, G.; Zheng, Z.; Wu, Y.; Feng, N. *Ceram. Int.* **2009**, *35*, 1-5.
36. Huang, M.; Xu, C.; Wu, Z.; Huang, Y.; Lin, J.; Wu, J. *Dyes Pigments* **2008**, *77*, 327-334.
37. Tian, J.; Wang, J.; Dai, J.; Wang, X.; Yin, Y. *Surf. Coat. Tech.* **2009**, *204*, 723-730.
38. Wang, C.; Wang, X.; Xu, B.; Zhao, J.; Mai, B.; Peng, P.; Sheng, G.; Fu, J. *J. Photoch. Photobio. A* **2004**, *168*, 47-52.
39. Zhang, M.; An, T.; Hu, X.; Wang, C.; Sheng, G.; Fu, J. *Appl. Catal. A: Gen.* **2004**, *260*, 215-222.
40. Seftel, E.; Popovici, E.; Mertens, M.; Stefaniak, E.; Van Grieken, R.; Cool, P.; Vansant, E. *Appl. Catal. B: Environ.* **2008**, *84*, 699-705.
41. Wang, H.; Baek, S.; Lee, J.; Lim, S. *Chem. Eng. J.* **2009**, *146*, 355-361.
42. Chen, T.; Zheng, Y.; Lin, J.; Chen, G. *J. Am. Soc. Mass Spectr.* **2008**, *19*, 997-1003.
43. Wang, Z.; Chen, H.; Tang, P.; Mao, W.; Zhang, F.; Qian, G.; Fan, X. *Colloids Surfaces A* **2006**, *289*, 207-211.
44. El Rehim, S.; Fouad, E.; El Wahab, S.; Hassan, H. *J. Electroanal. Chem.* **1996**, *401*, 113-118.
45. Kim, S.; Choi, J. *Electrochem. Commun.* **2008**, *10*, 175-179.
46. Sreekantan, S.; Hazan, R.; Lockman, Z. *Thin Solid Films* **2009**, *518*, 16-21.